LAWRENCE
LIVERMORE
NATIONAL
LABORATORY

LLNL-JRNL-664157

Multi-dimensional Vlasov simulations and Modeling of trapped-electron-driven filamentation of electron plasma waves

R. L. Berger, S. Brunner, J. W. Banks , B. I. Cohen, B. J. Winjum

November 11, 2014

Physics of Plasmas

Disclaimer

Multi-dimensional Vlasov simulations and Modeling of trapped-electron-driven filamentation of electron plasma waves

R. L. Berger[1],* S. Brunner[2],† J. W. Banks[3], B. I. Cohen[1], and B. J. Winjum[4]
(1) Lawrence Livermore National Laboratory, University of California, P.O. Box 808, Livermore, California 94551
(2) Centre de Recherches en Physique des Plasmas, Association Euratom-Confédération Suisse, Ecole Polytechnique Fédérale de Lausanne, CRPP-PPB, CH-1015 Lausanne, Switzerland
(3) Department of Mathematical Sciences, AE 301,110 8th Street, RPI, Troy, NY 12180, and
(4) Department of Electrical Engineering UCLA, Los Angeles, CA,
(Dated: January 14, 2015)

Kinetic simulations of two-dimensional finite amplitude Electron Plasma Waves (EPWs) are performed in a one-wavelength long system. A systematic study of the most unstable linear sideband mode, in particular its growth rate γ and wavenumber k_y, is carried out by scanning the amplitude and wavenumber of the initial wave. Simulation results are compared with numerical and analytical solutions to a two-dimensional nonlinear Schroedinger model [H. A. Rose and L. Yin, Phys. Plasmas **15**, 042311 (2008)] and to the reduced model by Kruer [W. L. Kruer *et al.*, Phys. Rev. Lett. **23**, 838 (1969)] generalized to two dimensions.

PACS numbers:

I. INTRODUCTION

A number of plasma instabilities, such as electron beam-plasma interactions and stimulated Raman scattering, may produce in the nonlinear state large amplitude electron plasma waves. In weakly collisional plasmas, such waves may evolve to a quasi-steady Bernstein-Greene-Kruskal (BGK)-like state.[1] In one dimension (1D), such waves are unstable to longitudinal sideband instabilities.[2] In two dimensions (2D), these waves undergo a transverse modulational instability akin to filamentation with a growth rate dependent on the number of trapped electrons.[3, 4] Here, we present 2D +2V (two dimensions in configuration and velocity space) Vlasov simulations of freely propagating large-amplitude EPWs for a range of wave amplitudes ϕ_L and wavenumbers $k_L\lambda_{De}$ and compare the results to a published theoretical model[5, 6] and to a new model, a herein derived generalization of the Kruer, Dawson and Sudan (GKDS) model [2] to multiple dimensions. This GKDS model considers also the growth of sidebands composed of Fourier modes with wavevectors at oblique angles to the wavevector $\vec{k}_L$ of the large amplitude EPW, in particular *transverse* sidebands with Fourier modes having wavevectors $\vec{k}_S = n\vec{k}_L + \delta\vec{k}_S$, $\delta\vec{k}_S \perp \vec{k}_L$, leading to filamentation instabilities. Landau damping of the obliquely propagating EPWs sets an amplitude-dependent limit on the magnitude of the largest unstable transverse wavenumber.

The filamentation of EPWs caused by a spatially varying nonlinear frequency produced by the presence of trapped and nearly trapped resonant particles was predicted based on a nonlinear Schroedinger equation model by Rose and Yin.[5, 7] Here, we analyze a similar but simpler model based on an extension to 2D of a model proposed by Dewar, [8] which we refer to as the Dewar-Rose-Yin (DRY) model. In its simplest form, this model predicts a growth rate that scales with $\phi_L^{1/2}$ whereas the Vlasov simulations presented here show a somewhat stronger scaling with ϕ_L but also a dependence on $k_L\lambda_{De}$. Given the remarkable success of the KDS dispersion in modeling the growth rate of the longitudinal TPI, [9] we extended that theory to 2D. A detailed derivation is given in Appendix A. In the limit that the bulk plasma response is treated in the fluid limit (consistent with the longitudinal TPI model), the solution of the dispersion relation involves finding the roots to an 8^{th} order polynominal with real coefficients. In this model, unstable roots are found at much larger transverse wavenumbers and with much larger growth rates than found in our Vlasov simulations. The DRY model is presented in Section III A and the generalized KDS model (GKDS) in Section III B. The growth rates of the GKDS model are brought into better agreement with the simulations by considering the effect of Landau damping. For waves traveling in the same direction as the initial wave and with phase velocities falling within the trapped region, Landau damping is strongly reduced. However, waves that propagate at finite angles to $\vec{k}_L$ experience a stronger gradient in the velocity distribution, that is, the damping is anisotropic and dependent

*berger5@llnl.gov
†stephan.brunner@epfl.ch

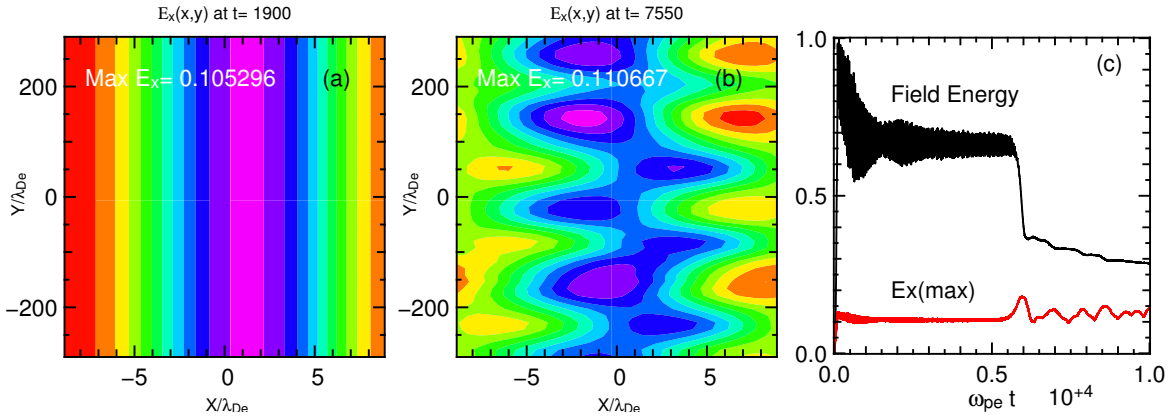

FIG. 1: Evolution of a plane wave from (a) its initial uniform transverse profile to (b) a filamented profile. (c) the time evolution of the total field energy (black) normalized to the maximum value and the maximum value of E_x (red). The electric field is normalized to $T_e/(e\lambda_{De})$.

on ϕ_L. A model for that anisotropic damping is developed in Sec. III C and applied to the DRY and GKDS growth rates in Sec. III D where reasonable agreement of the modified theory with the simulations is achieved. We conclude in Sec. IV.

II. SIMULATION RESULTS

In this section, we present simulation results obtained with LOKI [11] which solves the full 2D+2V nonlinear Vlasov-Poisson system, using an Eulerian based approach. The time and length scales are normalized to the inverse of the plasma frequency, $\omega_{pe} = \sqrt{N_e e^2/m_e\epsilon_0}$, and the electron Debye length, $\lambda_{De} = v_{\rm th,e}/\omega_{pe}$, where N_e is the electron plasma density, $v_{\rm th,e} = \sqrt{T_e/m_e}$ is the electron thermal velocity, T_e is the electron temperature, $-e$ is the electron charge, and m_e is the electron mass. These spatially two-dimensional simulations involve, in a first phase, generation of a large amplitude traveling plane wave (LAW), driven by the external potential ϕ^{ext} along the x direction with y taken as the transverse direction. In the second phase, the undriven wave breaks-up through the longitudinal trapped particle instability (TPI) and transverse filamentation instability. The longitudinal sideband instability has been studied thoroughly with 1D Vlasov simulations and the growth rates were shown to agree very well with the 1D KDS model.[9] In that case and here, the external field drives a wave to large amplitude over a short time, typically $\omega_{pe}t = 100$ after which an apparent quasi-stationary state is established. In the early part of the second stage after the external field is turned off, there are noticeable bounce oscillations in wave amplitude as the trapped electrons and the field exchange energy. Later, during the quiescent period, the mode frequency and trapped particle distribution function are measured and agree very well with an 'adiabatic' distribution[6] and its corresponding frequency shift as discussed in detail in Ref. [12]. The longitudinal instability involves growth of sideband EPWs with $|\delta\vec{k}_S| = |\vec{k}_S - \vec{k}_L| < |\vec{k}_L|$ which requires a system many wavelengths long along the propagation direction. That study in Ref. ([9]) imposed periodic boundary conditions along the x direction.

Here, we study transverse perturbations with perpendicular wavevector $\delta\vec{k}\perp\vec{k_L}$ and $|\delta k| = |k_y| \ll k_L$. The system is periodic in both spatial dimensions. To restrict the study to transverse instabilities only, the simulation is only one EPW wavelength long in the propagation direction. Typically, the simulation width is $192\pi\lambda_{De}$; the length is 6π for $k_L\lambda_{De} = 1/3$ and 4.71π for $k_L\lambda_{De} = 0.425$. For $k_L\lambda_{De} = 1/3$, an example is given in Fig. 1. During the apparently quiescent period from $t = 600\ \omega_{pe}^{-1}$ to $t = 5000\ \omega_{pe}^{-1}$, transverse perturbations grow exponentially until the peaks in the field amplitude localized in the transverse direction become apparent as shown in Fig. 1b. At this time, the electric field amplitude attains local maxima but the primary LAW is destroyed and much of the EPW field energy is converted to kinetic energy of electrons as shown in Fig. 1c.

In Fig. 2a, the time dependence of the 2D spatial Fourier transform of the field $|E_x(k_x = k_L, k_y)|$ shows exponential growth of 'sidebands' with ($\vec{k_S} = [k_L, k_y]$) to the primary wave ($\vec{k_L} = [k_L, 0]$). At the time the sideband amplitudes near the amplitude of the primary wave, a sudden loss in EPW field energy occurs with a sudden and equal gain in electron kinetic energy. The exponential growth of the fastest growing modes is shown in Fig. 2b and Fig. 2c on log and linear scales respectively.

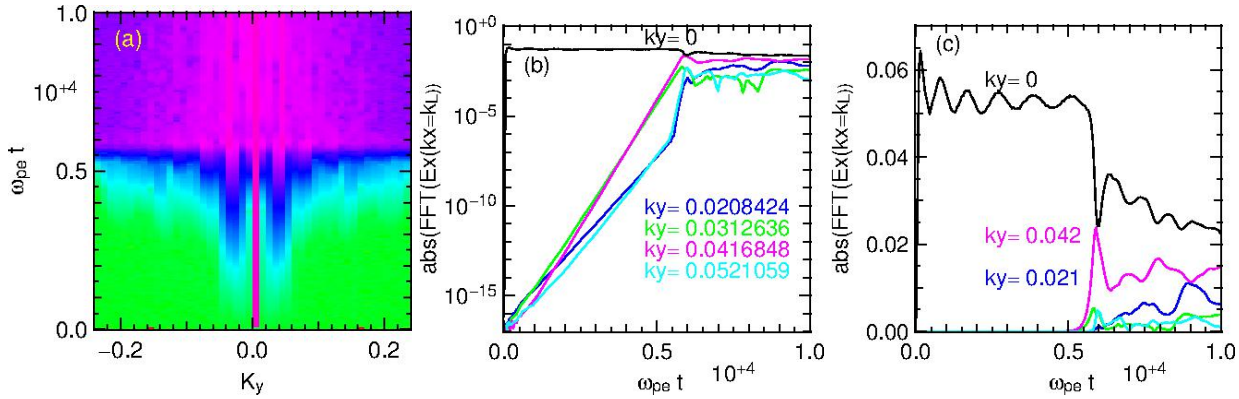

FIG. 2: (a) The magnitude of the Fourier transform of the field $|E_x(k_L, k_y)|$: shown is the log of $|E_x|$ versus k_y and time. (b) The exponential growth of transverse Fourier modes over 12 orders of magnitude. (c)The same as (b) but on a linear scale.

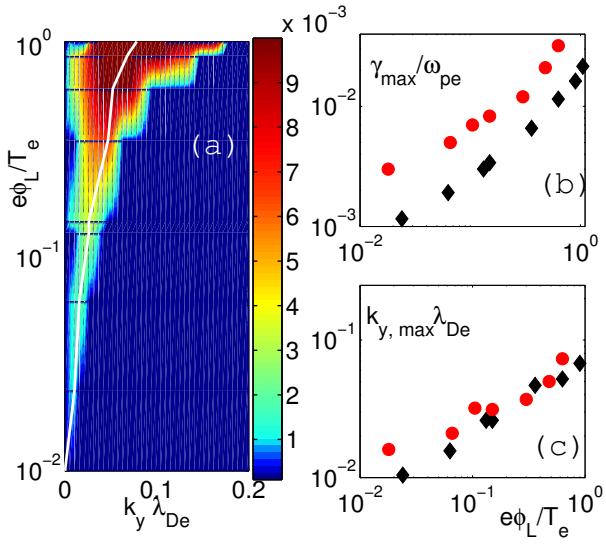

FIG. 3: Simulations: (a) The growth rate of the transverse modulations as a function of $k_y\lambda_{De}$ and the wave amplitude $e\phi_L/T_e$ where $k_L\lambda_{De} = 1/3$. (b) The maximum growth rate as a function of $e\phi_L/T_e$ for $k_L\lambda_{De} = 1/3$ (black) and $k_L\lambda_{De} = 0.425$ (red). (c) The wavenumber $k_{y,max}$ at which the growth rate is maximum as a function of $e\phi_L/T_e$ for $k_L\lambda_{De} = 1/3$ (black) and $k_L\lambda_{De} = 0.425$ (red).

Simulations have been done for an extensive scan of wave amplitudes from $e\phi_L/T_e = 0.01$ to $e\phi_L/T_e = 1$ for different values of $k_L\lambda_{De}$, and growth rates as a function of transverse wavenumber k_y extracted. The results are shown in Fig. 3. In Fig. 3a, the growth rate 'spectrum' is shown for the case where $k_L\lambda_{De} = 1/3$ as a function of the transverse wavenumber, $k_y\lambda_{De}$, and wave amplitude ϕ_L in the 'quiescent' period of evolution. In this plot, the white line traces out for each amplitude ϕ_L the wavenumber $k_{y,max}$ of the mode with the fastest growth rate, γ_{max}. In Fig. 3b,c, the maximum growth rate and the wavenumber $k_{y,max}$ of the mode with the fastest growth rate are plotted as a function of the wave amplitude $e\phi_L/T_e$ for both $k_L\lambda_{De} = 1/3$ and $k_L\lambda_{De} = 0.425$. Note for a given wave amplitude, the growth rate of the filamentation instability is faster for the higher wavenumber as one might expect given that the phase velocity is lower ($v_\phi = 3.1v_{\rm th,e}$ versus $v_\phi = 3.6v_{\rm th,e}$) and more electrons are trapped. Frequency analysis of the growing modes showed that they are filamentation-like with the same real frequency as the LAW. We note here for comparison to theoretical models that the maximum growth rate, γ_{max}, scales with wave amplitude as $\gamma_{max} \propto \phi_L^{2/3}$ for $k_L\lambda_{De} = 1/3$ but $\gamma_{max} \propto\sim \phi_L^{1/2}$ for $k_L\lambda_{De} = 0.425$ for $e\phi/T_e < 0.6$ above which the scaling is faster. However, the wavenumber of the fastest growing mode, $k_{y,max} \propto \phi_L^{1/2}$, scales with the square root of the wave amplitude.

III. THEORETICAL MODELS FOR EPW FILAMENTATION DRIVEN BY TRAPPED ELECTRONS

Here, in Sec. III A, we analyze a simple model for the filamentation instability based on an extension to 2D of a modulational instability developed by Dewar.[8] In its simplest form, the growth rate scales with $\phi_L^{1/2}$ whereas the Vlasov simulations show a faster scaling with ϕ_L. In Sec. III B, the KDS dispersion for the longitudinal TPI is generalized to 2D. Representing the bulk plasma response by the fluid limit (consistent with the longitudinal TPI model in Ref. ([9])), the solution of the GKDS dispersion relation involves finding the roots to an 8^{th} order polynominal with real coefficients. Unstable roots are found at much larger transverse wavenumbers and with much larger growth rates than found in the Vlasov simulations. The growth rates of the GKDS model are brought into better agreement with the simulations by considering the effect of Landau damping. For waves traveling in the same direction as ϕ_L with phase velocities falling within the trapped region, Landau damping is strongly reduced. However, as waves propagate at larger and larger angles to $\vec{k_L}$, they see a stronger gradient in the velocity distribution, that is, the damping is anisotropic and dependent on ϕ_L. A model for that damping is developed in Sec. III C and applied to the DRY and GKDS growth rates in Sec. III D.

A. Nonlinear Schroedinger Equation Model for EPW Filamentation

The filamentation of EPWs is predicted by a nonlinear Schroedinger equation proposed in Ref. [5, 7] which is an extension to 2D of a 1D model that leads to a longitudinal modulational instability.[8] In its simplest formulation that employs the fluid dispersion of EPWs, the model equation for the slow space and time variation of the envelope $\phi_k(x,y,t)$ of the full field, $\phi(x,y,t) = 1/2(\phi_k(x,y,t)\exp(i\vec{k}\cdot\vec{x} - i\omega_k t) + c.c.)$, is:

$$i\left(\frac{\partial}{\partial t} + \frac{\partial\omega_k}{\partial k_x}\frac{\partial}{\partial x} + \nu\right)\phi_k + \left(\frac{1}{2}\frac{\partial^2\omega_k}{\partial k_y^2}\frac{\partial^2}{\partial y^2} + \frac{1}{2}\frac{\partial^2\omega_k}{\partial k_x^2}\frac{\partial^2}{\partial x^2} + \Delta\omega\right)\phi_k = 0 \tag{1}$$

where the frequency shift $\Delta\omega \propto \sqrt{|\phi_L|}$ and ω_k is obtained by solving the dispersion relation $\epsilon(\vec{k},\omega) = 0$. As a first approximation for the dielectric function $\epsilon(\vec{k},\omega)$, the fluid relation (including thermal corrections) is used,[10]

$$\epsilon(\vec{k},\omega) = \epsilon(k,\omega) = 1 - \frac{\omega_{pe}^2}{\omega^2 - 3k^2 v_{\mathrm{th,e}}^2}, \tag{2}$$

where $k = |\vec{k}|$. Setting $k_y = 0$ yields Dewar's 1D model. The influence of including damping or using other coefficients from a kinetic dispersion relation are discussed in Secs. III D and in the conclusions. Here, we restrict perturbations to the transverse direction, neglect the damping ν, and, similar to Rose [5, 7], find a purely growing instability in the wave frame. Evaluating the dispersion by Taylor expanding ω_k about $\omega_L, k = k_L$, we find, $\partial^2\omega_k/\partial k_y^2 = 3v_{\mathrm{th,e}}^2/\omega_L$. The complex root, Ω, is

$$\Omega^2 \;=\; \frac{k_y^2}{4}\frac{\partial^2\omega_k}{\partial k_y^2}\left(\Delta\omega + k_y^2\frac{\partial^2\omega_k}{\partial k_y^2}\right). \tag{3}$$

If the RHS of Eq. (3) is positive, as it is for all k_y if $\Delta\omega > 0$, Ω is real. Otherwise, all $k_y < \left[|\Delta\omega|/(\partial^2\omega_k/\partial k_y^2)\right]^{1/2}$ are unstable. The maximum growth rate and the transverse wavenumber of the mode with the maximum growth are:

$$\gamma_m^{DRY} \;=\; \frac{|\Delta\omega|}{4} \tag{4}$$

$$K_m^{DRY} \;=\; \left|\frac{\Delta\omega}{2\frac{\partial^2\omega_k}{\partial k_y^2}}\right|^{1/2} \tag{5}$$

Here, $\Delta\omega$, the frequency shift for a large-amplitude EPW,

$$\frac{\Delta\omega}{\omega_{pe}} = -\frac{\alpha_e}{\sqrt{2\pi}(k_L\lambda_{De})^2}\sqrt{\frac{e\phi_L}{T_e}}\,(\mathsf{v}^2-1)\exp(-\frac{\mathsf{v}^2}{2})\Big|_{\mathsf{v}=v_\phi/v_{\mathrm{th,e}}}, \tag{6}$$

where $v_\phi = \omega_L/k_L$, has been found to be well represented by an adiabatic distribution of trapped electrons for which $\alpha_e = 0.544$.[6, 12] Using Eq. (6) in Eqs. (4) and (5), we find $\gamma_m^{DRY} \propto \phi_L^{1/2}$ and $K_m^{DRY} \propto \phi_L^{1/4}$. This DRY growth rate will be compared with that predicted by the generalized KDS model (GKDS) and the simulations in the following sections.

B. Generalization of the Sideband KDS Model to Multiple Dimensions

The derivation of the Kruer, Dawson and Sudan (KDS) model [2, 9] for the sideband instability is generalized here to multi-dimensions, i.e. for arbitrary orientation of wavevectors $\vec{k}_S$ with respect to the wavevector k_L of the LAW. The KDS model provides a linear stability analysis of a large-amplitude, periodic EPW to small-amplitude electrostatic fluctuations resulting from electron charge oscillations. The unperturbed system is thus non-homogeneous but periodic along the direction of propagation of the initial LAW. The linear eigenmodes resulting from this stability analysis are therefore Floquet (or Bloch) -type modes, which in general are each composed of a superposition of Fourier modes with wavenumbers $\vec{k}_S = n\vec{k}_L + \delta\vec{k}_S$, $n = 0, \pm1, \pm2, \ldots$. The general theory for the stability analysis of LAW's has been derived by Goldman[13]. The KDS model, an approximate derivation of Goldman's dispersion relation, assumes that the LAW significantly affects only the trapped particles dynamics. In the KDS model it is thus the trapped electrons which couple the Fourier modes in the Floquet-type eigenmodes and are the origin of their destabilization. In Appendix A, the generalized KDS dispersion relation (A16) is derived and written here explicitly for the special case of *transverse sidebands*, for which $|k_x| = k_L$ and $k_y \neq 0$, (filamentation-like), with the notation $k^2 = k_L^2 + k_y^2$ and $\vec{k}_L = k_L\vec{e}_x$ where $\vec{e}_{x,y}$ are unit vectors in the x, y directions respectively.

$$\epsilon(\vec{k},\omega)\,\epsilon(\vec{k}-2\vec{k}_L,\omega-2\omega_L) = \frac{\omega_t^2}{k^2}\left(\frac{k_L^2}{\Omega^2-\omega_B^2}+\frac{k_y^2}{\Omega^2}\right)\left[\epsilon(\vec{k},\omega)\ +\epsilon(\vec{k}-2\vec{k}_L,\omega-2\omega_L)\right] - \frac{4\omega_t^4}{\Omega^2(\Omega^2-\omega_B^2)}\frac{k_L^2k_y^2}{k^4}. \quad (7)$$

The right hand side of Eq. (7) clearly reflects the coupling of the Fourier modes by the trapped particles through the trapped electron plasma frequency squared, $\omega_t^2 = N_t e^2/(m\epsilon_0)$ where N_t is spatially averaged density of trapped particles. In the case of *longitudinal sidebands*, for which $k_y = 0$, Eq. (7) recovers the dispersion relation in the original KDS model restricted to longitudinal modes [Eq. (7) in reference [2]]. With use of Eq. 2, the dispersion relation (7) can be reduced to a polynomial equation for ω with real coefficients, so that the eigenmode frequencies are either real or appear in complex conjugate pairs. In the case of longitudinal sidebands, the corresponding dispersion relation reduces to a polynomial equation of degree 6, while both the purely transverse and the general sideband case, the former characterized by Eq. (7), reduce to a polynomial equation of degree 8.

1. *Numerical Solution to the GKDS and DRY Dispersion Relations*

Here, numerical solutions to the GKDS dispersion relation [Eq. (7)] for sidebands of EPWs are presented where Eq. (2) is used for $\epsilon(\vec{k},\omega)$. We consider a LAW with wavenumber $\tilde{k}_L = k_L\lambda_{De} = 1/3$, the same normalized wavelength as in Refs. [14] and [4] where wavefront bowing and self-focusing of two-dimensional EPWs with finite transverse width were studied. The numerical solution to the linear kinetic dispersion relation for an EPW with wavenumber $k\lambda_{De} = 1/3$, i.e. solving $\epsilon(\vec{k},\omega) = 0$ with the kinetic dielectric function, yields the real frequency $\omega_r/\omega_{pe} = 1.200$ (as well as damping rate $\gamma/\omega_{pe} = 2.587\cdot10^{-2}$) such that the phase velocity $v_\phi/v_{\rm th} = 3.6$. In contrast, the Bohm-Gross estimate obtained with the fluid relation (2) for the dielectric function, yields $\omega_r/\omega_{pe} = 1.155$ and the phase velocity $v_\phi/v_{\rm th} = 3.465$. In the GKDS model, both the normalized bounce frequency ω_B/ω_{pe} and density of trapped particles N_t/N_e are functions of ϕ_L. The bounce frequency ω_B/ω_{pe} is taken as the frequency of deeply trapped particles $\omega_{B,\rm deep}/\omega_{pe} = (e\phi_L/T_e)^{1/2}k_L\lambda_{De}$. The number of trapped electrons is computed for an adiabatic distribution of trapped electrons at a phase velocity of $3.6v_{\rm th,e}$ in agreement with the simulation results discussed in Sec. II for the transverse instabilities and in Appendix A of Ref. ([9]) for longitudinal instabilities.

The most unstable roots for the GKDS dispersion have a double-humped structure as a function of k_y which reflects the fact that there are two different types of unstable modes: a pair of sidebands displaced symmetrically around the frequency of the LAW and one with real frequency equal to that of the LAW (*i.e.*, a purely growing mode in the wave frame). The root related to the second hump remains unstable up to the relatively large value $k_y\lambda_{De} \simeq 0.58$. Fig. 4 shows the growth rate for a two-dimensional scan over both the normalized wavenumber $k_y\lambda_{De}$ and wave amplitude $e\phi_L/T_e$ for both the DRY model, Eq. (3) [Fig. 4b], and the GKDS model, Eq. (7) [Fig. 4a]. For Eq. (3) and (7), the most unstable growth rate $\gamma_{\rm max}$ has been identified at each amplitude ϕ_L, together with the corresponding transverse wavenumber $k_{y,\rm max}$. Both $\gamma_{\rm max}/\omega_{pe}$ and $k_{y,\rm max}\lambda_{De}$ have been plotted as a function of $e\phi_L/T_e$ for both dispersion models in Fig. 4c and Fig. 4d respectively. As $\phi_L \to 0$, the unstable roots and the transverse wavenumber of the unstable roots all vanish. For the DRY model, that behavior is obvious from Eqs. (4) and (6). In the dissipation-free GKDS dispersion relation, the instability persists in the limit $\omega_B < \omega_t$ for which $\phi_L < 1\times10^{-3}$. In that limit, straightforward analytic analysis shows that the growth rate and wavenumber of maximum growth are zero for $\phi_L = 0$. At this level of analysis, the simulation results are better represented by the DRY model than the GKDS model.

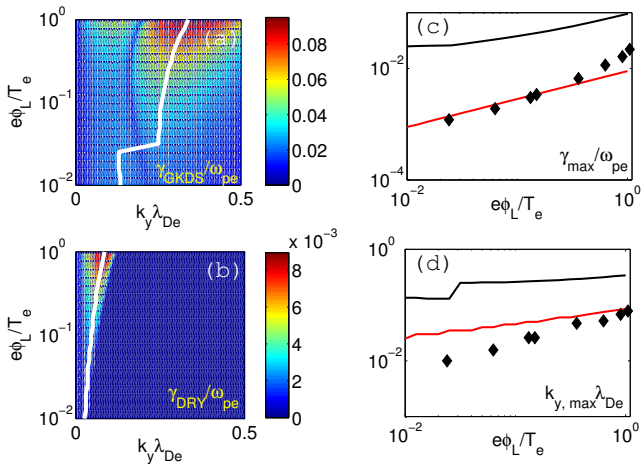

FIG. 4: The growth rate γ is shown as a function of the transverse wavenumber $k_y\lambda_{De}$ and amplitude $e\phi_L/T_e$. The fraction of trapped particles $N_t(\phi_L)/N_e$ is estimated for an 'adiabatic' distribution of trapped electrons and the bounce frequency $\omega_B(\phi_L) = \omega_{B,\mathrm{deep}}$. (a) Solution to the KDS dispersion relation for transverse sidebands. Notice the two humps, corresponding to two separate unstable branches. (b) Solution to the DRY dispersion relation. For each amplitude ϕ_L in (a) and (b), the wavenumber $k_{y,\mathrm{max}}$ has been identified at which the growth rate is maximum, leading to the curve plotted in white. (c) The maximum growth rate and (d) the wavenumber at the maximum growth rate respectively for the KDS and the DRY models in solid black and red lines respectively. The simulation results are shown by diamond markers.

C. Amplitude-Dependent Anisotropic Landau Damping

The two models, represented by Eqs. (3) and (7), take no account of the Landau damping rates. Here, we present a model that takes account of the modification of the Landau damping for a distribution that has been flattened by the LAW for all v_y and $v_\phi - v_{tr} < v_x < v_\phi + v_{tr}$ where the trapped electron velocity $v_{tr}/v_{\mathrm{th,e}} = 2\sqrt{e\phi_L/T_e}$.[15] The LAW equilibrium distribution function in two velocity dimensions is represented in the separable form:

$$f_0(\vec{v}) = N_e f_{0,x}(v_x) f_{0,y}(v_y), \tag{8}$$
$$f_{0,y}(v_y) = f_M(v_y), \tag{9}$$
$$f_{0,x}(v_x) = f_M(v_x) + \delta f_x^{flat}(u), \tag{10}$$
$$\delta f_x^{flat}(u) = P(u)\frac{1}{\sqrt{2\pi}v_{\mathrm{th,e}}}\exp(-\frac{u^2}{2}), \tag{11}$$
$$P(u) = \beta u + \gamma(u^2 - 1), \tag{12}$$
$$u = (v_x - v_{\phi,L})/\delta v, \tag{13}$$

where $f_M(v_{x,y}) = (1/(\sqrt{2\pi}v_{\mathrm{th,e}}))\exp(-v_{x,y}^2/(2v_{\mathrm{th,e}}^2))$ is a one-dimensional Maxwell-Boltzmann. The parameter, δv, represents the plateau width of the flattened region centered around $v_{\phi,L}$. Note, $\int dv_x \delta f_x^{flat}(u) = 0$ so δf_x has no effect on the total number of particles. Imposing the condition that the 1^{st} and 2^{nd} derivatives of $f_{0,x}(v_x)$ at the phase velocity, $v_x = v_{\phi,L}$, are zero determines the coefficients β and γ

$$\beta = (\delta\tilde{v})\bar{v}\exp(-\bar{v}^2/2)|_{\bar{v}=v_{\phi,L}/v_{\mathrm{th,e}}}, \tag{14}$$
$$\gamma = \frac{\delta\tilde{v}}{3}\left(1-\bar{v}^2\right)\exp(-\bar{v}^2/2)|_{\bar{v}=v_{\phi,L}/v_{\mathrm{th,e}}}, \tag{15}$$

where $\delta\tilde{v} = \delta v/v_{\mathrm{th,e}}$. In our calculations, $\delta v = v_{tr}$. It can be shown that the dielectric function for the distribution in Eq. (8) is

$$\epsilon(\tilde{\vec{k}},\tilde{\omega}) = 1 + \frac{1}{\tilde{k}^2}\left[W(\tilde{\omega}/\tilde{k}) + \Omega(\tilde{\vec{k}},\tilde{\omega})\right], \tag{16}$$
$$\Omega(\tilde{\vec{k}},\tilde{\omega}) = \frac{\delta v}{v_{\mathrm{th,e}}}\frac{\tilde{k}_x\tilde{k}^2}{\tilde{\kappa}^3}\left[Q\ W(z') + \left(\gamma\frac{\tilde{\kappa}_x}{\tilde{\kappa}} + \frac{\beta}{z'}\right)\right], \tag{17}$$

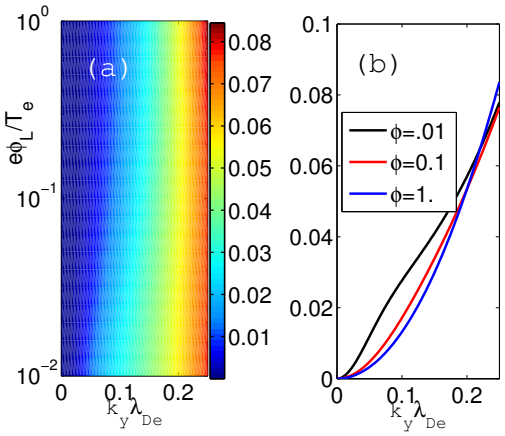

FIG. 5: (a) color contour plot the Landau damping rate divided by the plasma frequency, ν_{LD}/ω_{pe}, as a function of the wave amplitude, $e\phi_L/T_e$ and the transverse wavenumber, $k_y\lambda_{De}$;(b) ν_{LD}/ω_{pe} as a function of $k_y\lambda_{De}$ for three values of $e\phi_L/T_e$

with

$$Q \;=\; \left(\gamma\frac{\tilde{\kappa}_x}{\tilde{\kappa}}z'^2+\beta z'-3\gamma\frac{\tilde{\kappa}_x}{\tilde{\kappa}}-\frac{\beta}{z'}\right), \tag{18}$$

where $\tilde{k}=(\tilde{k}_x^2+\tilde{k}_y^2)^{1/2}$, $\tilde{\kappa}=(\tilde{\kappa}_x^2+\tilde{k}_y^2)^{1/2}$, $\tilde{\kappa}_x=\tilde{k_x}\delta\tilde{v}$, and $z'=(\tilde{\omega}-\tilde{k}_x v_{\phi,L}/v_{\rm th,e})/\tilde{\kappa}$. In Eq. (16), $W(\xi)=1+\xi Z(\xi)$ is the plasma dispersion function for a Maxwell-Boltzmann velocity distribution.

Of particular interest to the transverse filamentation instability is the Landau damping of a mode with real frequency $\omega_R\simeq\omega_L$ and $\vec{k}=k_L\vec{e}_x+k_y\vec{e}_y$ for the flattened distribution. That is shown in Fig. 5. For $k_y=0$, the damping $\nu_L=0$ as it must be by design. As k_y increases, the damping increases as well such that for large enough k_y it becomes the same as the Landau damping for an isotropic Maxwell-Boltzmann (MB) for a wave with the same phase velocity. For larger wave amplitudes, larger k_y is needed for the wave to be out of the plateau region of the distribution and experience the full Landau damping of the MB distribution. Note, the damping rate for $k_y\sim k_L$ is much larger than the damping of a wave with the same phase velocity, namely, $.026\omega_{pe}$ as the LAW propagating at a large angle to $\vec{k}_L$ because its phase velocity is smaller, *i.e.*, $\omega_L/\sqrt{k_L^2+k_y^2}$.

D. Growth Rates with Amplitude-Dependent Anisotropic Landau Damping subtracted

Comparison of the growth rates in Fig. 4 with the damping rates in Fig. 5 makes clear that the damping will reduce or even stabilize the growth for $k_y\lambda_{De}>0.2$. For the DRY model, keeping the damping term, ν in the analysis is done easily with the result that $\gamma\to\gamma+\nu$ such that the growth rate is simply reduced by ν. In general that is not possible for the GKDS model because the coupled modes have different wavenumbers and frequencies. However, for the special case considered here where only two sidebands $\vec{k}_\pm=\pm k_L\vec{e}_x+k_y\vec{e}_y$ are kept such that $|\vec{k}_+|=|\vec{k}_-|$, the damping rates of the two sidebands are equal if the frequencies are equal. In Fig. 4a, the frequencies of the both sidebands are the same for the branch with the larger k_y. Thus, with damping the already-obtained growth rates for the DRY and larger k_y GKDS modes without damping simply are reduced by the damping rate. For the other branch of GKDS modes with smaller k_y, the sideband frequencies are slightly upshifted and downshifted from ω_L such that *linearly* they have different damping rates. We have approximated their damping rates by using ω_L for both sidebands, a small error if $\nu_u+\nu_l\gg|\nu_u-\nu_l|$ where ν_u and ν_l are the damping rates of the upper and lower sideband respectively.

In Fig. 6, the growth rates shown are simply the growth rates shown in Fig. 4 with the damping rates in Fig. 5 subtracted. Now, the growth rates from both theories are in reasonable agreement with the simulation data shown in Fig. 3. The wavenumber of maximum growth is reduced, especially for the GKDS model, because of the strong Landau damping of the large k_y modes. The comparison of the GKDS and DRY models with the simulations is shown in Fig. 7 for both $k_L\lambda_{De}=1/3$ and $k_L\lambda_{De}=0.425$. The data is bracketed by the models, DRY on the low and GKDS

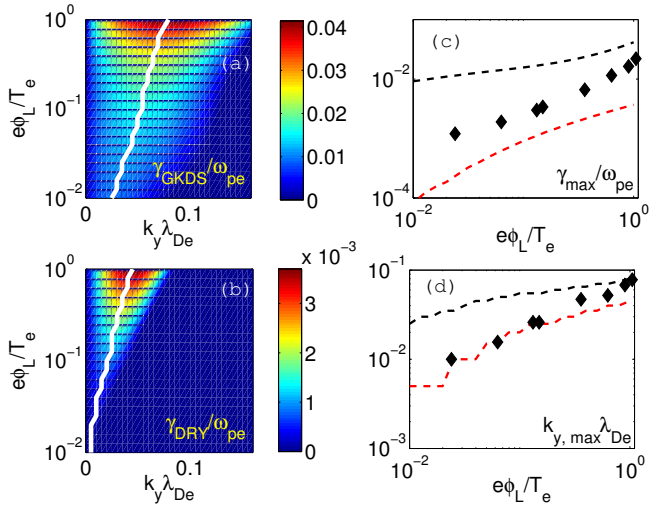

FIG. 6: The growth rates for the (a)GKDS and the (b) DRY models for $k_L\lambda_{De} = 1/3$ adjusted for the damping rates shown in Fig. 5. (c) The maximum adjusted growth rates for each model and the simulation results as a function of $e\phi_L/T_e$. (d) The wavenumber of the mode with maximum adjusted growth rates for each model and the simulation results as a function of $e\phi_L/T_e$.

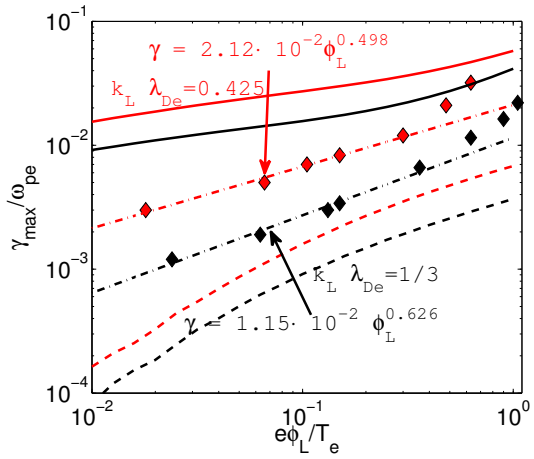

FIG. 7: The maximum growth rate of the filamentation instability from the simulations and the DRY [dashed curves] and GKDS [solid curves] models with damping included for $k_L\lambda_{De} = 1/3$ [black] and $k_L\lambda_{De} = 0.425$ [red]. The diamond markers are the results from the simulations for $k_L\lambda_{De} = 1/3$ [black diamonds] and $k_L\lambda_{De} = 0.425$ [red diamonds]. A power law fit to the simulation data is shown with dash-dot curves labeled with the equations that fit the data, again $k_L\lambda_{De} = 1/3$ [black] and $k_L\lambda_{De} = 0.425$ [red].

on the high side, for both LAW wavenumbers. A power law fit to the simulation data shows a $\phi^{2/3}$ dependence for $k_L\lambda_{De} = 1/3$ and a $\phi^{1/2}$ dependence for $k_L\lambda_{De} = 0.425$ except at the largest amplitudes.

IV. CONCLUSIONS

The Kruer-Dawson-Sudan (KDS) model [2], originally derived for analyzing the stability of large amplitude EPWs to longitudinal sideband instabilities [so-called Trapped Particle Instabilities (TPI)], has been generalized to multiple dimensions, leading to a new GKDS model that allows for the stability analysis of Fourier modes with transverse wavevector components as well (leading to so-called filamentation instabilities). The solutions to the KDS model and

the DRY nonlinear Schroedinger model, both using the fluid dielectric for the bulk plasma response were compared to simulation results for the flamentation instability obtained from the LOKI [11] code that solves the nonlinear Vlasov-Poisson system for EPWs. In previous treatments, these models have not included Landau nor collisional damping of the modulationally unstable longitudinal and transverse modes. For cases of practical interest, collisional damping is unimportant although collisional detrapping might be. The unstable longitudinal sidebands (see Ref. [9]) have phase velocities that fall in the region of velocity space flattened by the LAW. Thus, neglect of Landau damping of these sideband modes is justified. As we showed in Sec. III C, modes propagating at oblique angles to the LAW may be strongly damped at a rate dependent on their angle with respect to the LAW and on the LAW amplitude. Thus, their stability must be considered in this light as done here for the first time.

In case of the stability analysis of an EPW with wavenumber $k_L\lambda_{De} = 1/3$, the comparison shows qualitative agreement (i.e. scaling with respect to $e\phi_L/T_e$) for both the growth rate $\gamma_{\max}$ of the most unstable transverse sideband mode and associated transverse wavenumber $k_{y,\max}$ as a function of the normalized wave amplitude in the range $0.01 < \phi_L < 1$ provided one accounts for the Landau damping of obliquely propagating sidebands. We believe that this is the first direct and successful comparison of 2D Vlasov simulations results to the predictions of reduced theoretical models. The best agreement for the $k_L\lambda_{De} = 1/3$ case was achieved when solving the KDS or DRY model using the 'adiabatic' estimate for the fraction of trapped particles N_t/N_e (actually confirmed when directly diagnosing the trapped electron fraction and nonlinear frequency shift in the simulation) and evaluating the bounce frequency as $\omega_B = \omega_{B,\text{deep}}$. For the $k_L\lambda_{De} = 0.425$ case, the nonlinear frequency shift computed from the simulations follows the same scaling as Eq. (6) but with the larger coefficient $\alpha_e = 0.83$ appropriate for the 'sudden' approximation. Using that larger coefficient for the $k_L\lambda_{De} = 0.425$ case leads to a 20% increase in the maximum DRY growth rate (over that shown in Fig. 7)and a 10% increase in the DRY wavenumber for the maximum growth (before accounting for damping).

These theoretical models could be improved by a kinetic treatment of the distribution functions such that the nonlinear modification of the EPW frequency and damping is naturally taken into account. For the DRY model, kinetic modification of the dispersion, frequency shift, and damping are straightforward. Improving the GKDS model is more daunting as the energy dependence of the bounce frequency and the wavenumber and frequency dependence of the damping rates are nontrivial to include. However, the GKDS model already works very well for longitudinal sidebands whereas the DRY model does not. Because the physically relevant case (currently under study) has both instabilities at play with modes propagating at oblique angles, an improved GKDS model is clearly of interest.

It is interesting to compare quantitatively the growth rates obtained from the simulations for both the longitudinal sideband instability[9] to the ones obtained here for the transverse filamentation instability. That is done in Fig. 8. Note the filamentation and TPI sideband growth rates scale with the wave amplitude as $\phi^{2/3}$ for $k_L\lambda_{De} = 1/3$. In the KDS theory, the maximum sideband growth rate scales as the 1/3 power of the wave amplitude if $N_t \propto \sqrt{\phi_L}$. However, at the larger wave amplitudes, $\phi_L > 0.1$, $N_t \propto \phi_L$ in the simulations. With this scaling, one finds $\gamma_{max}^{TPI} \propto \phi_L^{1/2}$ well within the range of the simulation data.

V. ACKNOWLEDGEMENTS

We are pleased to acknowledge valuable discussions with T. Chapman, I. Dodin, D. Pesme, W. Rozmus, and L. Yin. This work was performed under the auspices of the U.S. Department of Energy by Lawrence Livermore National Laboratory under Contract DE-AC52-07A27344 and funded by the Laboratory Research and Development Program at LLL under project tracking code 12-ERD-061. Computing support for this work came from the Lawrence Livermore National Laboratory (LLL) Institutional Computing Grand Challenge program. B. J. Winjum acknowledges support from DOE under Grant No. DE-NA0001833.

Appendix A: Derivation of the Eigenvalue Equation for the Generalized KDS model

Consider the dynamics of a macro-particle trapped in the n'th potential well of a periodic EPW with wavevector $\vec{k}_L$. Let x be the direction of propagation of the EPW, and y the transverse direction. Introduce the corresponding unitary vectors $\vec{e}_x$ and $\vec{e}_y$, so that $\vec{e}_x \| \vec{k}_L$ and $\vec{e}_y \perp \vec{k}_L$. The position of such a particle is written $\vec{x}_n(t) = \vec{x}_{n0} + \vec{v}_{\phi,L}t + \vec{\xi}_n(t)$, where $\vec{v}_{\phi,L} = \omega_L/k_L\,\vec{e}_x$ is the phase velocity of the LAW, $\vec{x}_{n0} = x_{n0}\,\vec{e}_x + y_{n0}\,\vec{e}_y$ the unperturbed particle position in the wave frame, and $\vec{\xi}_n(t) = \xi_{x,n}(t)\,\vec{e}_x + \xi_{y,n}(t)\,\vec{e}_y$ its deviation. Clearly $x_{n0} = n\lambda_L$, with $n = 0, \pm1, \pm2, \ldots$ and $\lambda_L = 2\pi/k_L$ the wavelength of the EPW.

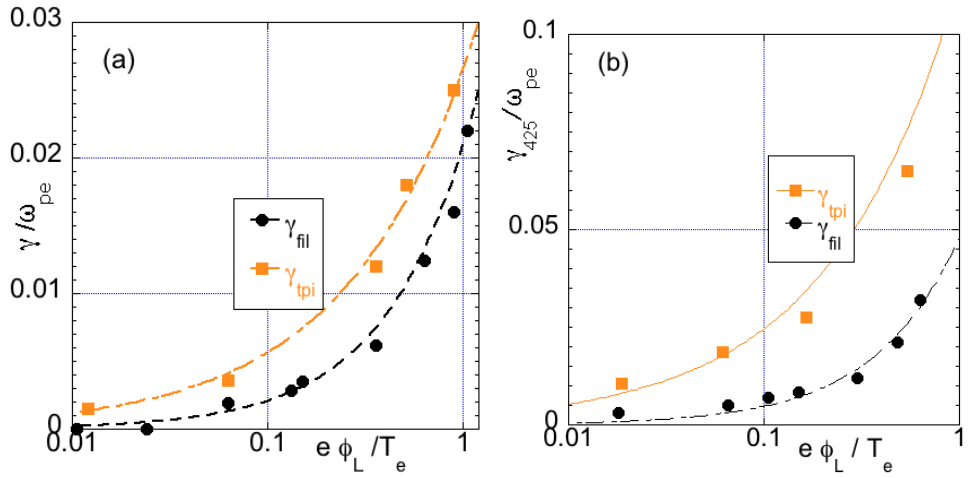

FIG. 8: The maximum growth rates of the longitudinal sideband instability [obtained in Ref. ([9])] and the transverse filamentation instability are shown as a function of ϕ_L for (a) $k_L\lambda_{De} = 1/3$ and (b) $k_L\lambda_{De} = 0.425$. In both cases of k_L, the longitudinal sideband instability has a faster growth rate than the transverse filamentation instability. For equal wave amplitude, ϕ_L, the growth rates are larger for larger k_L because of the increased number of trapped electrons.

Newton's equation of motion along x of a trapped macro-particle in the presence of sidebands is written:

$$\frac{d^2}{dt^2}\xi_{x,n}(t) = -\omega_B^2\,\xi_{x,n}(t) - \frac{e}{m_e}E_x[\vec{x}_n(t),t], \tag{A1}$$

where $\omega_B/\omega_{pe} = (e\phi_L/T_e)^{1/2}k_L\lambda_{De}$ is the deeply-trapped-electron bounce frequency for an EPW with wave amplitude ϕ_L. Here E_x is the electric field component along x. Consistent with the linearization procedure, $E_x[\vec{x}_n(t),t] \simeq E_x[\vec{x}_{n0}+\vec{v}_{\phi,L}t,t]$. Furthermore, the sideband field $\vec{E}(x,t)$ derives from an electrostatic potential $\phi(x,t)$, $\vec{E} = -\partial\phi/\partial\vec{x}$, which can be represented in general as a superposition of Fourier modes:

$$\phi(x,t) = \int d\vec{k}d\omega\,\phi(\vec{k},\omega)\exp[i(\vec{k}\cdot\vec{x}-\omega t)].$$

The solution to Eq. (A1) can thus be written:

$$\xi_{x,n}(t) = -\frac{e}{m_e}\int d\vec{k}d\omega\,\frac{ik_x\phi(\vec{k},\omega+k_xv_{\phi,L})}{\omega^2-\omega_B^2}\exp[i(\vec{k}\cdot\vec{x}_{n0}-\omega t)]. \tag{A2}$$

Similarly, the equation of motion along the transverse direction y reads:

$$\frac{d^2}{dt^2}\xi_{y,n}(t) = -\frac{e}{m_e}E_y[\vec{x}_n(t),t], \tag{A3}$$

where $E_y = -\partial\phi/\partial y$ is the sideband electric field component along y. Note that the motion along y is unconstrained by the LAW potential. The corresponding solution is given by

$$\xi_{y,n}(t) = -\frac{e}{m_e}\int d\vec{k}d\omega\,\frac{ik_y\phi(\vec{k},\omega+k_xv_{\phi,L})}{\omega^2}\exp[i(\vec{k}\cdot\vec{x}_{n0}-\omega t)]. \tag{A4}$$

One can now derive the charge density $\rho_n(\vec{x},t)$ associated to a single macro-particle:

$$\rho_n(\vec{x},t) = -e\,\delta[\vec{x}-\vec{x}_n(t)] = -e\,\delta\Big[\vec{x}-\Big(\vec{x}_{n0}+\vec{v}_{\phi,L}t+\vec{\xi}_n(t)\Big)\Big],$$

where $\delta(\vec{x})$ is the Dirac distribution. For small amplitude sideband fluctuations, a Taylor expansion is valid and leads to

$$\rho_n(\vec{x},t) \simeq -e\,\delta\left[\vec{x}-(\vec{x}_{n0}+\vec{v}_{\phi,L}t)\right] + e\,\vec{\xi}_n(t)\cdot\frac{\partial}{\partial\vec{x}}\delta\left[\vec{x}-(\vec{x}_{n0}+\vec{v}_{\phi,L}t)\right]. \tag{A5}$$

The first term on the right hand side of Eq. (A5) is the unperturbed part of the charge density, a source component to the electrostatic field of the LAW, while the second term is the fluctuating part $\tilde{\rho}_n(\vec{x},t)$:

$$\tilde{\rho}_n(\vec{x},t) = e\,\vec{\xi}_n(t)\cdot\frac{\partial}{\partial\vec{x}}\delta\left[\vec{x}-(\vec{x}_{n0}+\vec{v}_{\phi,L}t)\right]. \tag{A6}$$

The fluctuation component of the total trapped electron charge density $\tilde{\rho}_t(\vec{x},t)$ can then be written:

$$\tilde{\rho}_t(\vec{x},t) = N_t\lambda_L\sum_{n=-\infty}^{+\infty}\int_{-\infty}^{+\infty} dy_{n0}\,\tilde{\rho}_n(\vec{x},t), \tag{A7}$$

integrating over all possible unperturbed transverse positions y_{n0} of the trapped particles and summed over all potential wells of the LAW indexed by n. The Fourier transform of the fluctuating charge density is needed for the eigenvalue equation for the sideband modes and is conveniently written in Fourier space. By using Eq. (A6), the transform of $\tilde{\rho}_n(\vec{x},t)$ is found:

$$\begin{aligned}
\tilde{\rho}_n(\vec{k},\omega) &= \frac{1}{(2\pi)^3}\int d\vec{x}dt\,\tilde{\rho}_n(\vec{x},t)\exp[-i(\vec{k}\cdot\vec{x}-\omega t)]\\
&= \frac{e}{(2\pi)^3}i\vec{k}\cdot\int d\vec{x}dt\,\vec{\xi}_n(t)\\
&\quad\delta\left[\vec{x}-(\vec{x}_{n0}+\vec{v}_{\phi,L}t)\right]\exp[-i(\vec{k}\cdot\vec{x}-\omega t)]\\
&= \frac{e}{(2\pi)^3}\exp(-i\vec{k}\cdot\vec{x}_{n0})\\
&\quad i\vec{k}\cdot\int dt\,\vec{\xi}_n(t)\exp[i(\omega-k_xv_{\phi,L})t]\\
&= \frac{e}{(2\pi)^2}\exp(-i\vec{k}\cdot\vec{x}_{n0})\,i\vec{k}\cdot\vec{\xi}_n(\omega-k_xv_{\phi,L}),
\end{aligned} \tag{A8}$$

From Eqs. (A2) and (A4), one furthermore obtains:

$$\xi_{x,n}(\omega) = -\frac{e}{m_e}\int d\vec{k}\frac{ik_x\phi(\vec{k},\omega+k_xv_{\phi,L})}{\omega^2-\omega_B^2}\exp(i\vec{k}\cdot\vec{x}_{n0}), \tag{A9}$$

$$\xi_{y,n}(\omega) = -\frac{e}{m_e}\int d\vec{k}\frac{ik_y\phi(\vec{k},\omega+k_xv_{\phi,L})}{\omega^2}\exp(i\vec{k}\cdot\vec{x}_{n0}). \tag{A10}$$

Combining Eqs. (A7), (A8), (A9), and (A10), the Fourier transform of the total fluctuating trapped particle charge density becomes:

$$\begin{aligned}
\tilde{\rho}_t(\vec{k},\omega) &= N_t\lambda_L\sum_{n=-\infty}^{+\infty}\int_{-\infty}^{+\infty} dy_{n0}\,\tilde{\rho}_n(\vec{k},\omega)\\
&= \frac{N_t\lambda_Le}{(2\pi)^2}\sum_{n=-\infty}^{+\infty}\int_{-\infty}^{+\infty} dy_{n0}\,i\vec{k}\cdot\vec{\xi}_n(\omega-k_xv_{\phi,L})\exp(-i\vec{k}\cdot\vec{x}_{n0})\\
&= \frac{\lambda_L}{(2\pi)^2}\frac{N_te^2}{m}\int d\vec{k}'\sum_{n=-\infty}^{+\infty}\int_{-\infty}^{+\infty} dy_{n0}\,\exp[i(\vec{k}'-\vec{k})\cdot\vec{x}_{n0}]\times\\
&\qquad\left[\frac{k_xk_x'}{(\omega-k_xv_{\phi,L})^2-\omega_B^2}+\frac{k_yk_y'}{(\omega-k_xv_{\phi,L})^2}\right]\phi(\vec{k}',\omega+(k_x'-k_x)v_{\phi,L}).
\end{aligned}$$

Making use of relations

$$\int_{-\infty}^{+\infty} dy_{n0}\,\exp(ik_yy_{n0}) = 2\pi\delta(k_y),$$

$$\sum_{n=-\infty}^{+\infty}\exp(ik_xx_{n0}) = \sum_{n=-\infty}^{+\infty}\exp(ink_x\lambda_L) = k_L\sum_{n=-\infty}^{+\infty}\delta(k_x-nk_L),$$

leads to

$$\tilde{\rho}_t(\vec{k},\omega) = \frac{N_t e^2}{m}\sum_{n=-\infty}^{+\infty}\int dk'_x dk'_y \delta(k'_y - k_y)\delta[k'_x - (k_x + nk_L)]\times \left[\frac{k_x k'_x}{(\omega - k_x v_{\phi,L})^2 - \omega_B^2} + \frac{k_y k'_y}{(\omega - k_x v_{\phi,L})^2}\right]\phi(\vec{k}',\omega + (k'_x - k_x)v_{\phi,L})$$
$$= \frac{N_t e^2}{m}\sum_{n=-\infty}^{+\infty}\left[\frac{k_x(k_x + nk_L)}{(\omega - k_x v_{\phi,L})^2 - \omega_B^2} + \frac{k_y^2}{(\omega - k_x v_{\phi,L})^2}\right]\phi(k_x + nk_L, k_y, \omega + n\omega_L). \quad \text{(A11)}$$

The fluctuating trapped electron charge density $\tilde{\rho}_t$ appears as a source to Poisson's equation for the electrostatic potential associated to the sidebands, together with the corresponding bulk electron charge density response $\tilde{\rho}_b$:

$$-\triangle\,\phi(\vec{x},t) = \frac{1}{\epsilon_0}\left(\tilde{\rho}_b(\vec{x},t) + \tilde{\rho}_t(\vec{x},t)\right). \quad \text{(A12)}$$

In the KDS model, the bulk response is assumed to respond as in a homogenous plasma, i.e. with no modifications from the LAW and can thus be written in Fourier space as $\tilde{\rho}_b(\vec{k},\omega) = -k^2\epsilon_0\chi(\vec{k},\omega)\phi(\vec{k},\omega)$, where χ is the electric susceptibility of the homogenous plasma. Poisson's equation (A12) in Fourier space thus becomes:

$$k^2\left[1 + \chi(\vec{k},\omega)\right]\phi(\vec{k},\omega) = k^2\epsilon(\vec{k},\omega)\phi(\vec{k},\omega) = \frac{1}{\epsilon_0}\tilde{\rho}_t(\vec{k},\omega), \quad \text{(A13)}$$

where $\epsilon = 1 + \chi$ is the dielectric function of the homogenous plasma. Inserting Eq. (A11) into (A13) one finally obtains the linear system of equations for the Fourier mode components of the electrostatic potential field associated to the sidebands:

$$(k_x^2 + k_y^2)\epsilon(\vec{k},\omega)\phi(\vec{k},\omega) = \omega_t^2\sum_{n=-\infty}^{+\infty}\left[\frac{k_x(k_x + nk_L)}{(\omega - k_x v_{\phi,L})^2 - \omega_B^2} + \frac{k_y^2}{(\omega - k_x v_{\phi,L})^2}\right]\phi(k_x + nk_L, k_y, \omega + n\omega_L). \quad \text{(A14)}$$

As expected, the system of equations (A14) couples Fourier modes $\phi(\vec{k} + n\vec{k}_L, \omega + n\omega_L)$, $n = 0, \pm1, \pm2, \dots$, so that the corresponding eigenmodes are indeed of Floquet-type.

In reference [2], the analog of system (A14) coupling an infinite number of Fourier modes is reduced to the coupling of just two modes with the argument that the dominant Fourier components are the ones with frequency of the order of the electron plasma frequency ω_{pe}. The left hand side of Eq. (A14) provides the eigenvalue equation for plane EPWs with frequency $\omega \sim \omega_{pe}$, while the right hand side can be seen as a perturbation providing coupling between these EPWs through the electrons trapped in the initial LAW (naturally also an EPW with frequency $\omega_L \sim \omega_{pe}$). Thus, all the dominant Fourier modes composing the Floquet-type solution of the sideband are assumed to have frequency of order ω_{pe}. If the frequency of a certain Fourier mode $\phi(\vec{k},\omega)$ is such that $\omega \sim \omega_{pe}$ the only coupled mode with similar frequency (in absolute value) is $\phi(\vec{k} - 2\vec{k}_L, \omega - 2\omega_L)$. Therefore, in a first approximation, the coupled system is truncated to these two modes, which as a result reduces to the following rank 2 eigenvalue equation:

$$\mathbf{M}\cdot\begin{pmatrix}\phi(k_x,k_y,\omega)\\ \phi(k_x - 2k_L, k_y, \omega - 2\omega_L)\end{pmatrix} = 0, \quad \text{(A15)}$$

with

$$\mathbf{M} = \begin{pmatrix}(k_x^2 + k_y^2)\epsilon(0) - \omega_t^2\left(\frac{k_x^2}{\Omega^2 - \omega_B^2} + \frac{k_y^2}{\Omega^2}\right) & -\omega_t^2\left(\frac{k_x(k_x - 2k_L)}{\Omega^2 - \omega_B^2} + \frac{k_y^2}{\Omega^2}\right)\\ -\omega_t^2\left(\frac{k_x(k_x - 2k_L)}{\Omega^2 - \omega_B^2} + \frac{k_y^2}{\Omega^2}\right) & [(k_x - 2k_L)^2 + k_y^2]\epsilon(-2) - \omega_t^2\left(\frac{(k_x - 2k_L)^2}{\Omega^2 - \omega_B^2} + \frac{k_y^2}{\Omega^2}\right)\end{pmatrix},$$

with the notation $\epsilon(n) = \epsilon(k_x + nk_L, k_y, \omega + n\omega_L)$ as well as $\Omega = (\omega + n\omega_L) - (k_x + nk_L)v_{\phi,L} = \omega - k_x v_{\phi,L}$.

Equation (A15) thus defines an eigenvalue equation for the sidebands to the LAW. An eigenmode is thus composed of the two dominant Fourier modes $\phi(k_x, k_y, \omega)$ and $\phi(k_x - 2k_L, k_y, \omega - 2\omega_L)$ where the wavevector-frequency pair (k_x, k_y, ω) must satisfy the sideband dispersion relation,

$$\det(\mathbf{M}) = 0. \quad \text{(A16)}$$

For fixed $\vec{k} = (k_x, k_y)$, the determinant $\det(\mathbf{M})$ is in general an analytic function of the complex frequency ω. Solving the dispersion relation (A16) thus reduces to finding the zeroes of this analytic function. The dispersion relation (A16) can be written more explicitly as follows:

$$k_0^2\, k_{-2}^2\, \epsilon(0)\, \epsilon(-2) = \omega_t^2 \left[\left(\frac{k_{x,-2}^2}{\Omega^2 - \omega_B^2} + \frac{k_y^2}{\Omega^2} \right) k_0^2\, \epsilon(0) + \left(\frac{k_{x,0}^2}{\Omega^2 - \omega_B^2} + \frac{k_y^2}{\Omega^2} \right) k_{-2}^2\, \epsilon(-2) \right] - \frac{4\, \omega_t^4 k_L^2 k_y^2}{\Omega^2(\Omega^2 - \omega_B^2)}, \quad \text{(A17)}$$

with the notation $k_{x,n} = k_x + n k_L$ and $k_n^2 = k_{x,n}^2 + k_y^2$. The right hand side of Eq. (A17) reflects the coupling of the Fourier modes by the trapped particles through the factor ω_t^2.

[1] I. B. Bernstein, J.M. Green, and M. D. Kruskal, Phys. Review **108**, 546 (1957).
[2] W. L. Kruer, J. M. Dawson, and R. . Sudan, Phys. Rev. Lett. **23**, 838 (1969).
[3] L. Yin, B. J. Albright, H. A. Rose, K. J. Bowers, B. Bergen, D. S. Montgomery, J. L. Kline, and J. C. Fernandéz, Phys. Plasmas **16**, 113101 (2009).
[4] B. J. Winjum, R. L. Berger, T. Chapman, J. W. Banks, and S. Brunner, Phys. Rev. Lett. **111**, 105002 (2013).
[5] H. A. Rose and L. Yin, Phys. Plasmas **15**, 042311 (2008).
[6] R. L. Dewar, Phys. Fluids **15**, 712 (1972).
[7] H. A. Rose, Phys. Plasmas **12**, 012318 (2005).
[8] R. L. Dewar, W. L. Kruer, and W. M. Manheimer, Phys. Rev. Lett. **28**, 215 (1972).
[9] S. Brunner, R. L. Berger, B. I. Cohen, L. Hausammann and E. J. Valeo, Phys. Plasmas **21**, 102104 (2014).
[10] One could alternatively choose to expand about a kinetic solution to the linear dispersion. However, that requires a numerical solution to obtain the group velocity and the dispersion coefficients. In Ref. [12], we found that expansion about the Landau root worked well with a frequency shift that agreed well with Eq. (6) for both $k\lambda_{De} = 1/3$ and $k\lambda_{De} = 0.425$. Using an analytic form for the coefficients facilitates obtaining closed form expressions and the results will be seen to compare well with the simulation results.
[11] J. W. Banks and J. A. F. Hittinger, IEEE T. Plasma. Sci **38**, 2198 (2010)
[12] R. L. Berger, S. Brunner, T. Chapman, L. Divol, C. H. Still, and E. J. Valeo, Phys. Plasmas **20**, 032107 (2013).
[13] M. V. Goldman, Phys. Fluids **13**, 1281 (1970).
[14] J. W. Banks, R. L. Berger, S. Brunner, B. I. Cohen, and J. A. F. Hittinger, Phys. Plasmas **18**, 052102 (2011).
[15] This model is an extension to two dimensions of one used to model one dimensional kinetic simulations: L. Divol, E. A. Williams, B. I. Cohen, A. B. Langdon, and B. F. Lasinski, in Proceedings of the Third International Conference on Inertial Fusion Sciences and Applications (IFSA2003) (2003).